# A Design Methodology for Micromechanical Bandpass Filters

*Qi Jing*[†], *Tamal Mukherjee*[†], *Gary K. Fedder*[†*]
[†]Department of Electrical and Computer Engineering and [*]The Robotics Institute
Carnegie Mellon University, Pittsburgh, PA 15213-3890 USA
email: qjing@ece.cmu.edu

## Abstract

*A third-order high-Q 300 kHz micromechanical bandpass filter, with Q-adjustment and frequency tuning, is analyzed using a parameterized cell library, "NODAS," for schematic representation and behavioral HDL simulation. An equivalent SPICE model of the filter is derived, which enables simulation in SPICE and comparison to NODAS. Frequency response around the filter passband from NODAS simulation matches that from SPICE simulation to within 4%. Limitations of equivalent SPICE model are discussed. NODAS models have an advantage in simulating the effects of manufacturing variations, finite masses of beams, and actuator nonlinearity.*

**Keywords:**

**MEMS, micromechanical bandpass filter, nodal simulation, analog-HDL modeling**

## 1: Introduction

The bandpass filter is a key component of transceivers in communication technology. Popular physical implementations are based on mechanical devices such as crystal resonators, and electronic devices such as transistor LC circuits. Although IC technology enables integration, the performance of electronic filters is restricted by the limited quality factor of the electronics. Therefore, mechanical devices are more widely used, due to their distinguishing high quality factor. However, since mechanical devices are off-chip components, the interface with integrated electronics has to be at the board level, which becomes a crucial bottleneck for miniaturization and performance of transceivers [1].

CMOS micromachining technology provides a potential solution to this problem. High-Q mechanical resonators can be implemented on-chip [2] and integrated with electronic interface circuits, forming miniaturized, high-performance Microelectromechanical Systems (MEMS).

Micromechanical resonators fabricated in MEMS technology involve physical interactions between mechanical, electrostatic and fluidic domains. Design of bandpass filters composed of multiple resonators is a good example of the utility of MEMS CAD tools in designing such complex systems.

In the convention of mechanical bandpass filter design, the order of the filter is synonymous with the number of resonators. Higher order means more complexity in design. A filter using up to three resonators was first designed by Nguyen *et. al.* [1], using a linearized equivalent SPICE model as the design guide.

In this paper, we present a design methodology for micromechanical bandpass filters using NODAS. NODAS (Nodal Design of Actuators and Sensors) is a hierarchical cell library for nodal simulation of MEMS [3]. The NODAS cell library consists of symbols and behavioral models of elements commonly found in suspended MEMS design, such as beams, plates and electrostatic comb drives. These symbols can be wired together to quickly compose the resonator schematic. The resonator then serves as a building-block for higher level schematics of more complicated systems like filters. Each element in NODAS has a parameterized behavioral model, written in Verilog-A AHDL [4]. Simulation of the entire system is done using Spectre™.

The design of a third-order bandpass filter, which has a bandwidth of 760 Hz, and center frequency of 299.56 kHz, together with Q-adjustment and frequency tuning, is given as an example. A similar topology as in [1] is used as a starting point and for comparison. The filter topology is presented in Section 2. Using lumped parameter assumptions, equivalent linearized SPICE models for the filter are developed in Section 3. The frequency response of the filter is simulated in NODAS and compared with the simulation from the equivalent SPICE model. Section 4 then continues on detail simulation of non-ideality in the filter that cannot be captured in the equivalent SPICE model but can be obtained from NODAS, showing the advantage of using NODAS as the simulation tool.

## 2: Filter Topology

The third-order bandpass filter presented in this paper is composed of three identical folded-flexure resonators, each resonating at 299.43 kHz, coupled by flexural mode springs. The topology of the folded-flexure resonator is shown in Figure 1(a). When voltage is applied across the electrostatic comb drive, the suspended shuttle masses and flexural beams will move in *x* direction driven by the electrostatic force. The schematic of the entire filter is shown in Figure 1(b), together with the equivalent SPICE circuit, Q-adjustment and frequency tuning circuits.

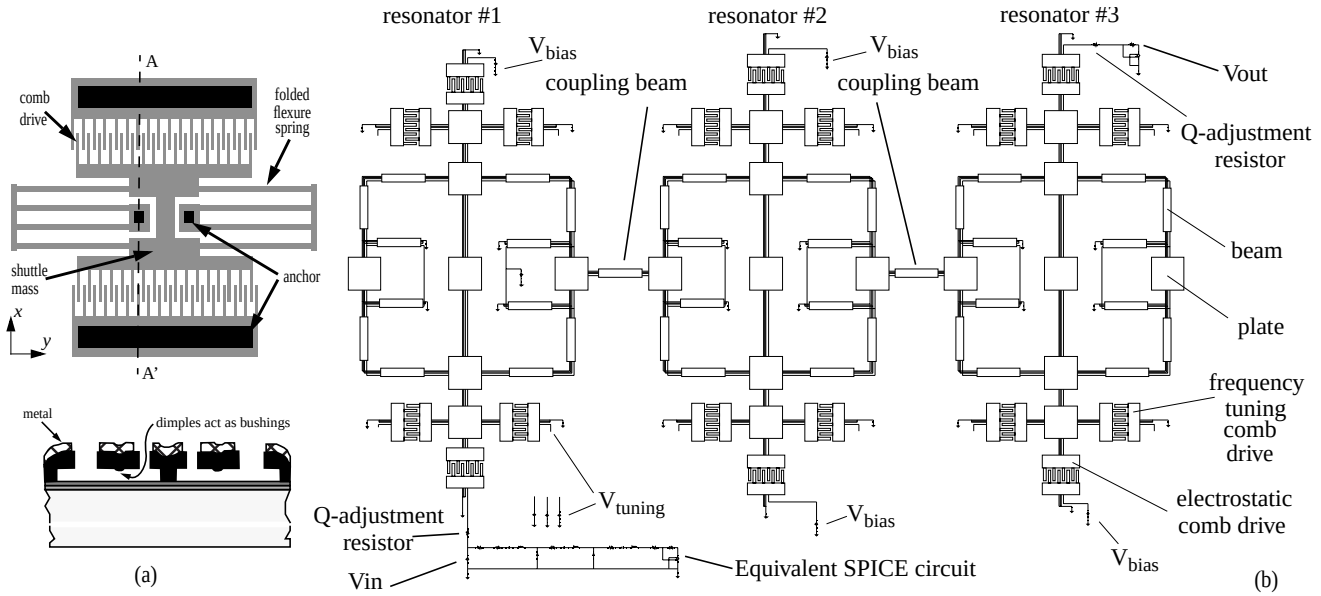


Figure 1: (a) Layout and cross view of a folded-flexure resonator, (b) Schematic of the third-order bandpass filter in Spectre

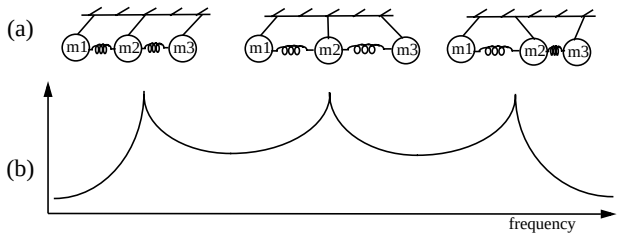


Figure 2: Diagram showing three modes(a) and peaks(b)

According to the analysis of coupled resonators [5], at the lowest natural frequency, all the resonators vibrate in phase, and at the highest natural frequency, all adjacent resonators vibrate 180 degrees out of phase. Each resonator adds an additional natural frequency to the system, and the resonances between the lowest and the highest natural frequencies have displacement patterns where a resonator maybe in phase, out of phase, or stationary with respect to its neighbor. The third-order bandpass micromechanical filter has three resonant modes, as shown in Figure 2(a). The three resonance peaks scatter around the resonance frequency of a single resonator, forming a passband shown in Figure 2(b). The location and spacing of the three peaks are determined by the stiffness of coupling beams, leading to different center frequency and bandwidth. The peaks can be flattened to form a flat passband by applying Q-adjustment techniques.

## 3: Linearized Equivalent SPICE Model

### 3.1: Circuit Analogy

The circuit analogies of second-order systems are commonly used. Representing the mechanical resonator as an ideal second-order system, composed of a lumped mass, a spring, and a damper, we can exploit this analogy to obtain a series or parallel equivalent circuit as shown in Figure 3.

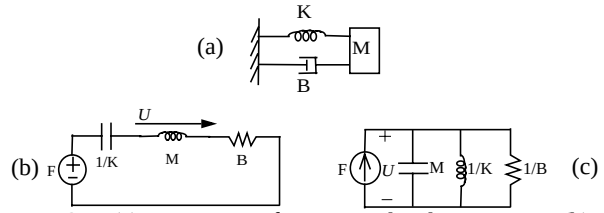


Figure 3: (a) Diagram of a second-order system, (b) Equivalent circuit (in series analogy), (c) Equivalent circuit (in parallel analogy)

### 3.2: Coupling Beams

The third-order filter is composed by coupling three resonators. We assume the coupling beams are massless, having ideal spring constants of $K_{12}$ and $K_{23}$ in the flexural mode. Under this assumption, the filter can be represented by a series of three second-order systems, coupled by ideal springs, as shown in Figure 4(a). Two kinds of equivalent capacitor networks are developed for the coupling beams, called I-type (Figure 4(b)) and T-type (Figure 4(c)).

The mechanical-electrical analogy can be seen in the transfer functions of the mechanical system (Figure 4(a)) in the frequency domain:

$$\left[M_1 s^2 + B_1 s + (K_1 + K_{12})\right] X_1(s) - K_{12} X_2(s) = F(s) \quad (1)$$

$$-K_{12} X_1(s) + \left[M_2 s^2 + B_2 s + (K_{12} + K_{23} + K_2)\right] X_2(s) - K_{23} X_3(s) = 0 \quad (2)$$

$$-K_{23} X_2(s) + \left[M_3 s^2 + B_3 s + (K_3 + K_{23})\right] X_3(s) = 0 \quad (3)$$

and the transfer functions of the electrical system (Figure 4(b), with I-type capacitor network) in the frequency domain:

$$\left[L_1 S + R_1 + \left(\frac{1}{SC_1} + \frac{1}{SC_{12}}\right)\right] I_1(S) - \frac{1}{SC_{12}} I_2(S) = V(S) \quad (4)$$

$$-\frac{1}{SC_{12}} I_1(S) + \left[L_2 S + R_2 + \left(\frac{1}{SC_2} + \frac{1}{SC_{12}} + \frac{1}{SC_{23}}\right)\right] I_2(S) - \frac{1}{SC_{23}} I_3(S) = 0 \quad (5)$$

$$-\frac{1}{SC_{23}} I_2(S) + \left[L_3 S + R_3 + \left(\frac{1}{SC_3} + \frac{1}{SC_{23}}\right)\right] I_3(S) = 0 \quad (6)$$

Applying the analogy shown in Table 1 to Eq (4)-(6), and comparing to Eq (1)-(3), we find that the coupling capacitors in the I-type network are:

$$C_{12} = 1/K_{12} \quad , \quad C_{23} = 1/K_{23},$$

where $K_{12}$ and $K_{23}$ is the equivalent spring constants of the coupling beams in flexural mode.

When using an I-type capacitor network, the equivalent RLC values are the same as those used in the equivalent series circuit for a single resonator (Figure 3). In our design, the three resonators are identical, and so are the two coupling beams. Thus, the I-type SPICE model reduces to: $R_1=R_2=R_3=R=B$, $L_1=L_2=L_3=L=M$, $C_1=C_2=C_3=C=1/K$, $C_{12} = C_{23} = C_{ij} = 1/K_{ij}$.

An alternative to the I-type topology is the T-type topology, which is similar to what is used in [1]. $C_1'$, $C_2'$, $C_3'$ , $C_a$, $C_b$ and $C_c$ in the T-type network (Figure 4(c)) can be related to $C_{ij}$ and $C$ of the I-type network by:

$$C_a = -C_b = -C_c = C_{ij}, C_1' = C_3' = \frac{C_{ij}C}{C_{ij}+C}, C_2' = \frac{C_{ij}C}{C_{ij}+2C} \quad .$$

### 3.3: Calculation of $K_{ij}$

The coupling structure shown in Figure 1 is a simple beam moving in the flexural mode. $K_{ij}$ is its spring constant for this particular mode shape, with guided-end boundary conditions at both ends. The coupling truss is displaced half as much as the shuttle mass in the filter structure shown in Figure 1 while the coupling spring is directly attached to the shuttle mass in the lumped parameter diagram of the filter (Figure 4(a)). We need to taken into account the difference in displacement when calculating $K_{ij}$:

The spring constant of a guided-end beam is:

Table 1. Analogy between mechanical and electrical domain

| **mechanical** | **electrical analogy** |
|---|---|
| across variable F(s) | across variable V(s) = F(s) |
| through variable U(s)=sX(s) | through variable I(s) = U(s) |
| mass = M | inductor = L = M |
| spring = K | capacitor = C = 1/K |
| damper = B | resistor = R = B |

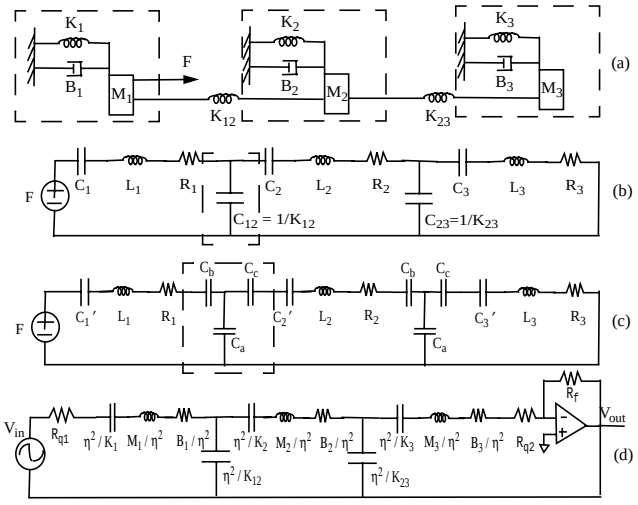


Figure 4: (a)Mechanical system with lumped parameters, (b) Equivalent circuit using I-type coupling network, (c) Equivalent circuit using T-type coupling network, (d) Equivalent circuit using T-type coupling network, modified by scaling factor η.

$k_0=Etw^3/l^3$, where $E$ is the Young's modulus, $t$ is the beam thickness, $w$ is the width, and $l$ is the length. Then

$K_{ij} = k_0/4, \quad C_{ij} = 1/K_{ij} = 4/k_0$ .

The coupling structure can be much more complicated than a single beam, in which cases the theoretical formula for a SPICE equivalent model may be difficult to obtain. In those cases, the effective spring constant can be obtained from simulation using either conventional finite element analysis, or NODAS.

### 3.4: The Electrostatic Comb Drive

As shown in Figure 1, the resonators are driven by electrostatic forces generated by comb drives. Since the SPICE model given in Figure 4(b) is for a pure mechanical structure only, a scaling factor, η, is determined to interface between the SPICE model and the electrical interface circuitry [6].

By assuming operation around resonance and neglecting static and second harmonic forces, the modified equivalent RLC equations are as follows:

$$C_x = \frac{\eta^2}{K} \qquad L_x = \frac{M}{\eta^2} \qquad R_x = \frac{\sqrt{KM}}{Q\eta^2} \qquad \eta = V_p \frac{\partial C_n}{\partial x}$$

where Q is the quality factor, $\partial C_n/\partial x$ is the change of comb drive capacitance per unit displacement in the $x$ direction at each stage, and $V_p$ is the bias voltage applied to the resonators.

An equivalent SPICE circuit with scaled parameters is shown in Figure 4(d). The interface circuitry (input driving circuit and output sensing circuit) can be combined together with the mechanical resonators, forming an equivalent SPICE model for the entire filter. The coupling capac-

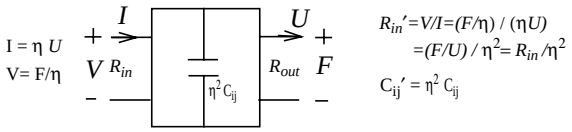


Figure 5: Scaling of coupling capacitor network

itor $C_{ij}$ is also scaled by a factor of $\eta^2$ since the through and across variables at the input and output of the coupling network have been scaled, as shown in Figure 5 .

## 4: Simulation Results

### 4.1: Simulation Using NODAS and SPICE Models

Figure 1 shows the filter schematic in NODAS, together with the SPICE equivalent circuit, which is magnified in Figure 4(d). Both circuits are driven by a common voltage source, but have separate sets of identical transresistance-amplifier sensing circuits.

As mentioned, the equivalent SPICE models represent the mechanical resonators as second-order systems of lumped parameters M, K and B, and represent the coupling beams as massless ideal springs with spring constant $K_{ij}$. Therefore, when we compare the simulations in NODAS and SPICE, all the beams in NODAS schematic are set to be massless. In reality, both flexural and coupling beams have finite masses. The finite-mass effect of beams will be discussed later.

Figure 6 shows the frequency response of the filter. The natural frequency of the resonators is 299.43 kHz, and the quality factor is 495,000. The coupling beams are 88.2 μm long and 1.12 μm wide. There are three peaks around the natural frequency, ranging from 299.43 kHz to 299.95 kHz. NODAS and SPICE results match to within 4%.

### 4.2: Q-adjustment

The resonant peaks can be reduced to form a flat passband for the filter by applying a Q-adjustment technique. Following [1], input and output series resistors to reduce Q of end resonators are added to both the NODAS and SPICE

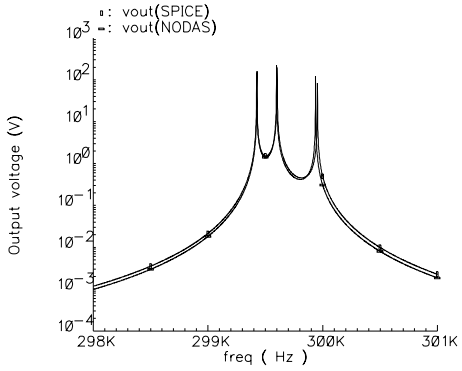


Figure 6: Frequency response of the filter (massless beams)

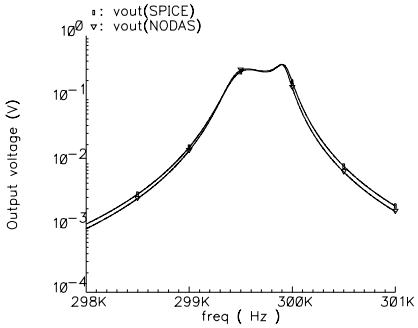


Figure 7: Frequency response with Q-adjustment

models as indicated in Figure 1. Figure 7 shows the frequency response of the filter after inserting the Q-controlling resistors. The three sharp peaks of the initial high-Q filter are now compressed down to a nearly flat passband with a ripple of -21dB (Q ≅ 587). NODAS and SPICE simulation results match to within 4%.

### 4.3: Finite-Mass Effect of Beams

The actual flexure and coupling beams are not ideal springs. The finite masses of flexure beams will shift the center frequency of the filter and thus affect coupling. The masses of coupling beams will add to the lumped parameter equivalent masses of adjacent resonators so as to shift resonant frequencies and cause passband distortion. Although the effect of flexure beam masses can be taken care of by using effective mass for this particular topology of folded-flexure resonators [1], it is difficult to find the effective mass for new resonator topologies, and even more difficult to represent the finite masses of coupling springs.

In NODAS, lumped parameter models are at the layout-based element-level (beams), instead of at device-level (resonators) as in equivalent SPICE model. Thus issues like finite mass of beams and velocity difference between shuttles and beams are inherently considered. Figure 8 shows the comparison of cases with and without masses of beams. The beam masses cause the center frequency to decrease.

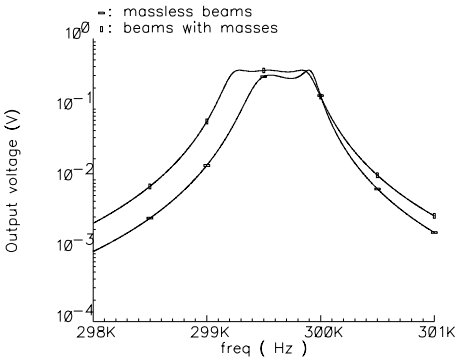


Figure 8: Finite-mass effect in frequency response

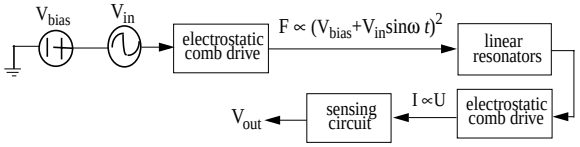


Figure 9: Nonlinearity of actuators

### 4.4: Nonlinear effects of actuators

The electrostatic comb drives exhibit a nonlinear effect since the electrostatic force generated by comb drives is proportional to the square of driving voltage, shown in Figure 9. For a sinusoidal driving voltage at frequency ω, the electrostatic force contains frequency terms at both ω and 2ω. The amplitude ratio of the fundamental force at ω to the second harmonic force at 2ω depends on the ratio of DC bias voltage to sinusoidal voltage amplitude.

The equivalent SPICE model does not capture this nonlinear effect. The scaling factor η used in the SPICE model is effective only when the DC bias voltage is much higher than the amplitude of AC voltage.

This nonlinearity is modeled directly in the electrostatic comb drive elements in NODAS. The transient analysis result includes all the existing frequency terms so that we can verify the existence of this nonlinearity.

Figure 10 shows the FFT of transient results. In order to see both frequency terms, the frequency of input sinusoidal voltage is set to half of the center frequency, and DC bias voltage is set to half of the sinusoidal amplitude, thus the amplitude of the 2ω term in the electrostatic force is

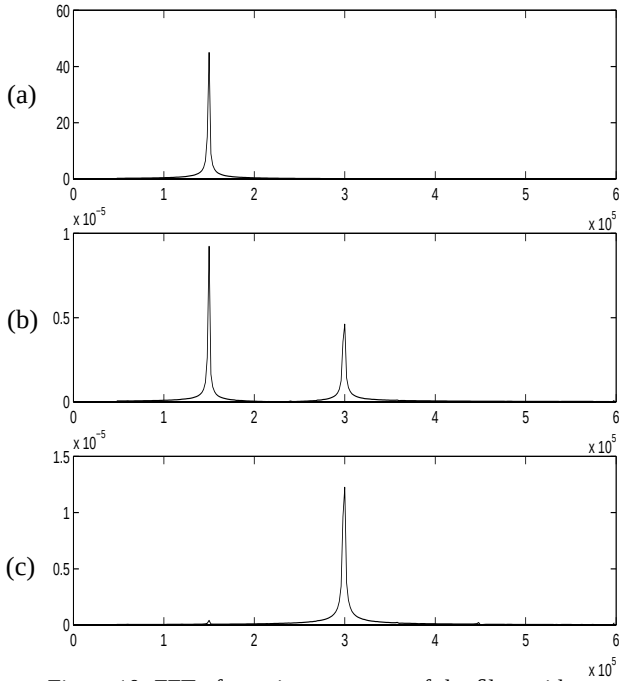


Figure 10: FFT of transient response of the filter with input sinusoidal voltage at 149.8 kHz, (a) Input sinusoidal voltage, (b) Electrostatic force generated by the comb drive, (c) Output voltage of the bandpass filter

half the amplitude of the ω term. The existence of the 2ω term in electrostatic force can be clearly seen (Figure 10(b)). Since the ω term is far outside of the passband, it is attenuated. The 2ω term falls into the passband, and is amplified. Therefore, the ω term is overwhelmed by the 2ω term at the output of the filter (Figure 10(c)).

### 4.5: Manufacturing Variations and Frequency Tuning

Another issue considered in this design is frequency tuning. There are many factors which can cause the shift of center frequency, change of bandwidth and distortion in the passband. The most common and inevitable nonideal factor is the manufacturing variation.

We model the manufacturing variations due to lithography and etching as a variation in the width of flexure and coupling beams. The small norminal widths of beams imply that manufacturing variation will affect them more significantly than other filter components. The layout value for the width of flexure beams ($w_b$) is 2 μm, and for the width of coupling beams ($w_c$) is 1.12 μm. Table 2 shows a set of values for $w_b$ and $w_c$, with random variations ranging from +0.04 μm to -0.30 μm (assuming matched variation in $w_b$ and $w_c$). Figure 11 shows the frequency response of the filter for those cases. All the beams are simulated with finite masses, for a more accurate representation of the system.

Table 2. Simulation data for manufacturing variations

| | Δw (μm) | $w_b$ (μm) | $w_c$ (μm) | $f_c$ (kHz) | BW (Hz) |
|---|---|---|---|---|---|
| 0 | 0 | 2.00 | 1.12 | 299.556 | 756 |
| 1 | +0.02 | 2.02 | 1.14 | 303.869 | 790 |
| 2 | +0.04 | 2.04 | 1.16 | 308.198 | 823 |
| 3 | -0.04 | 1.96 | 1.08 | 290.975 | 696 |
| 4 | -0.06 | 1.94 | 1.06 | 286.706 | 671 |
| 5 | -0.08 | 1.92 | 1.04 | 282.452 | 640 |
| 6 | -0.10 | 1.90 | 1.02 | 278.214 | 612 |
| 7 | -0.12 | 1.88 | 1.00 | 273.992 | 583 |
| 8 | -0.16 | 1.84 | 0.96 | 265.596 | 529 |
| 9 | -0.20 | 1.80 | 0.92 | 257.266 | 475 |
| 10 | -0.30 | 1.70 | 0.82 | 236.747 | 343 |

The width variation results in a center frequency variation ranging from 237 kHz to 308 kHz, and bandwidth ranging from 343 Hz to 823 Hz. The bandwidth is mainly determined by the spring constant of the coupling beams. The softer the coupling spring is, the weaker the coupling, therefore the smaller is the bandwidth.

In order to compensate for the manufacturing variation, a frequency tuning technique can be applied, as discussed in [1]. Tuning is implemented by including additional pairs of comb drives orthogonal to each resonator (Figure 1). Each pair of tuning comb drives is connected

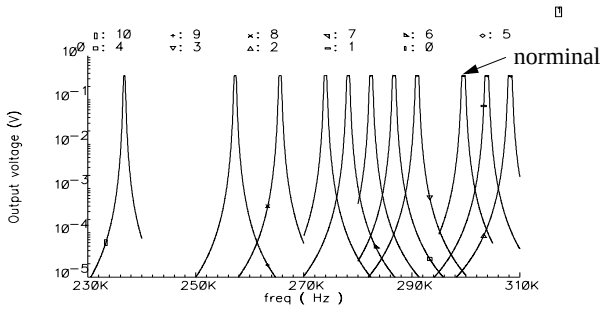


Figure 11: Filter frequency response with manufacturing variations

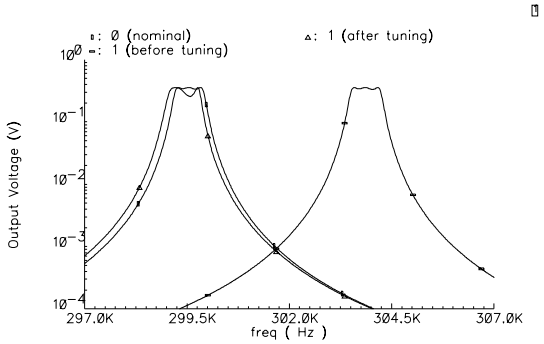


Figure 12: Using frequency tuning to correct passband shift due to manufacturing variation (test case is case1 as shown in Table 2, case 0 is the norminal case)

to its own DC tuning voltage. The electrostatic spring constants are dependent on tuning voltages due to the nonlinearity of comb drives, thus the resonant frequency of resonators can be tuned separately so as to correct the passband. Figure 12 shows that when there is a passband shift due to manufacturing variation, the center frequency can be corrected back to the designed region by applying a tuning voltage (85 Volts across the frequency tuning comb drives in this case).

## 5: Conclusions

A third-order high-Q micromechanical bandpass filter, centered at 299.56 kHz, with bandwidth of 760 Hz is designed, using NODAS for schematic representation and behavioral HDL simulation. Q-adjustment and frequency tuning techniques are applied and simulated.

Linearized equivalent SPICE models are developed for comparison of simulation against NODAS models. The results suggest that both models are good for modeling of the filter in restricted application regions. However, the equivalent SPICE model for the filter, which is a device-level lumped parameter model, has limitations in representing effects existing in real device elements, including finite-masses of beams, manufacturing variation, and actuator nonlinearity. These effects are directly modeled in the layout-based element-level lumped parameter behavioral models for beams and electrostatic comb drives in NODAS, therefore, they are analyzed and simulated, showing the advantage of using NODAS as a design tool. Moreover, NODAS cell library enables hierarchical simulation of systems more complicated than the bandpass filters, for which the equivalent SPICE models may be cumbersome to obtain.

## Acknowledgment

This research effort is sponsored by the Defense Advanced Research Projects Agency under the Air Force Research Laboratory, Air Force Material Command, USAF, under grant number F30602-96-2-0304 and in part by G.K.Fedder's National Science Foundation CAREER Award MIP-9625471.

## References

[1] K.Wang and C.T.-C. Nguyen, "High-Order Micromechanical Electronic Filters," *IEEE MEMS Workshop*, Japan, January 26-30, 1997, pp.25-30.

[2] W.C. Tang, T.-C.H. Nguyen, and R.T. Howe, "Laterally Driven Polysilicon Resonant Microstructures," *Sensor and Actuators* 20, pp.25-32, 1989.

[3] G.K. Fedder and Q. Jing, "A Hierarchical Circuit-Level Design Methodology for Microelectromechanical Systems," to be published in *IEEE Trans. on Circuits & Systems II*, 1999.

[4] Cadence Design Systems, Inc., 555 River Oaks Parkway, San Jose, California 95134, http://www.cadence.com

[5] R.A. Johnson, Mechanical Filters in Electronics, New York: John Wiley & Sons, 1983.

[6] C.T.-C.Nguyen, "Micromechanical Resonators for Oscillators and Filters", *Proc. 1995, IEEE International Ultrasonic Symposium*, Seattle, WA, pp. 489-499, Nov.7-10, 1995